RESEARCH ARTICLE | FEBRUARY 20 2025

Strain-engineering the lattice thermal conductivity of 2D kagome silica

Yang Wang; Xiaoying Wang; Yuzhou Hao; Xuejie Li; Yujie Liu; Jun Sun ; Xiangdong Ding ; Zhibin Gao

Appl. Phys. Lett. 126, 072202 (2025)
https://doi.org/10.1063/5.0253235

Applied Physics Letters ARTICLE pubs.aip.org/aip/apl

Strain-engineering the lattice thermal conductivity of 2D kagome silica

Cite as: Appl. Phys. Lett. **126**, 072202 (2025); doi: 10.1063/5.0253235
Submitted: 15 December 2024 · Accepted: 7 February 2025 ·
Published Online: 20 February 2025

Yang Wang, Xiaoying Wang, Yuzhou Hao, Xuejie Li, Yujie Liu, Jun Sun, Xiangdong Ding, and Zhibin Gao[a)]

AFFILIATIONS

State Key Laboratory for Mechanical Behavior of Materials, School of Materials Science and Engineering, Xi'an Jiaotong University, Xi'an 710049, China

[a)]Author to whom correspondence should be addressed: zhibin.gao@xjtu.edu.cn

ABSTRACT

Two-dimensional (2D) materials exhibit a significant potential for thermal management and thermoelectric energy generation due to their unique electrical and thermal transport properties that enhance performance. Their notable stretchability indicates the feasibility of employing strain engineering to optimize both electronic and thermal properties. In this study, we apply first-principles computational methods and the Boltzmann transport equation to explore the impact of strain and higher-order anharmonicity from four-phonon (4ph) scattering on the thermal conductivity (κ_L) of 2D silica. Our results indicate that under a small strain of 3%, κ_L increases due to the decrease in the phonon scattering rate and phonon phase space. However, under larger strains (8%), κ_L decreases significantly due to an increased phonon–phonon scattering rates. These findings provide deeper insights into the thermal transport behavior of 2D silica, paving the way for future research in strain and phonon engineering in 2D materials.

Silicon dioxide (silica), one of the most abundant materials in the Earth's crust, has attracted considerable research attention due to its significance in areas such as geology, microelectronics, and catalysis. In recent years, both experimental and theoretical studies have made substantial progress in the growth of ultra-thin silica films on metal single-crystal substrates, including Mo (112),[1] Ru (0001),[2] and graphene.[3,4] Additionally, advancements have been made in the detachment of 2D silica films from their growth substrates,[5] opening up new possibilities for exploring the atomic structure of 2D silica and its potential applications in mechanical,[6–8] electronic,[9–11] and crystalline-vitreous interfaces.[4,12]

2D silica features a kagome lattice structure composed entirely of rigid, interlocking triangles, which leads to an inherently unstable crystal configuration. Under lattice compression, this topological and mechanical instability causes the triangular units to rotate,[13] highlighting the substantial effect of strain on the structural stability and atomic interactions of 2D silica. The stability of the kagome lattice is significantly influenced by phonon–phonon interactions at finite temperatures, underscoring the essential role of anharmonic effects in the material's thermodynamic behavior.[14,15]

Strain and deformation commonly exist in 2D materials. When 2D materials are integrated into nanodevices, typically they are deformed due to constraints imposed during device assembly. On the other hand, strain engineering has also been proposed to tune electronic, photonic, and even thermal properties.[16,17] κ_L of 2D materials demonstrates significant strain dependence. For graphene, tensile strain can enhance or reduce κ_L, with the trend determined by sample size.[18,19] In pristine MoS_2 sheets, tensile strain markedly reduces thermal conductivity, primarily due to strain-induced strong anharmonicity and diminished phonon group velocities, as revealed by molecular dynamics simulations.[20,21]

When contemplating thermal transport properties, a potential overestimation of κ_L may occur in certain materials if the calculation solely accounts for the effects of third-phonon (3ph) anharmonicity. It is imperative to consider the influence of 4ph interactions.[22–24] Examples of such materials include silicon,[22] diamond,[24] arsenic boride allotropes,[25,26] graphene,[23] $TlAgI_2$,[27] Tl_9SbTe_6,[28] and perovskite.[29,30]

This study systematically analyzed κ_L of 2D silica under strains ranging from 0% to 8%, incorporating the contributions of 3ph and 4ph interactions and exploring the influences of heat capacity, phonon group velocity, phonon scattering rate, weighted phase space, and frequency shifts in dispersion relations. By applying biaxial tensile strain up to 8% to reflect its tunable thermal performance, 2D silica exhibits an increase in κ_L in the range of 0%–3% tensile strain, attributed to the decrease in phonon scattering rate and phonon phase space, which collectively outweigh the decrease in heat capacity. These competing

properties interact in a complex manner, causing a nonlinear increase in κ_L when tensile strain is applied. Under large-scale strains ranging from 3% to 8%, a significant decrease in κ_L is observed due to the elevated scattering rates.

DFT calculations were performed using the Vienna *ab initio* simulation package (VASP)[31] with the projector-augmented wave (PAW) method.[32,33] The PBE functional was employed to determine the lattice constants. Cutoff energy of 550 eV was used with $15 \times 15 \times 1$ Monkhorst–Pack k-grids. The self-consistent iteration for the energy convergence criterion was 10^{-8} eV, and all geometries were optimized by the conjugate-gradient method until none of the residual Hellmann–Feynman forces exceeded 10^{-4} eV/Å. We adopt our modified Alamode code[29,34] to output the renormalized anharmonic second-, third-, and fourth-order IFCs that are functions of the temperature and can be smoothly interfaced with the ShengBTE.[35] For 3ph and 4ph scatterings, we used a $40 \times 40 \times 1$ and $7 \times 7 \times 1$ q-mesh grids. Related theory and more calculation details can be found in previous works.[30,36]

In Figs. 1(a) and 1(b), the top and side views of the crystal structure of 2D-Si_4O_8 with *P6/mmm* symmetry are presented. Its primitive cell contains 4 silicon (Si) atoms and 8 oxygen (O) atoms with optimized lattice constants a = b = 5.312 Å. Within the planar bilayer, four neighboring oxygen atoms surround one silicon atom, forming standard sp^3 hybrid orbitals. From the top view, 2D silica possesses a kagome lattice that is composed of rigid triangles, which has many exotic properties such as surface phonons[13,15] and topological phases for non-abelian braiding.[37] Since the intrinsic twisted mode of the kagome model, lattice compression would lead to the rotation of the triangular units, indicating the significance of the instability[15] of phonon and anharmonicity[38,39] in the thermodynamics state.

Figures 1(c) and 1(d) illustrate the structural changes in 2D-Si_4O_8 under applied strain, presenting the functional relationships between tensile strain and lattice constants, bond lengths, and bond angles. Upon the application of biaxial strain, the nanocage undergoes expansion, leading to a linear increase in the lattice constant (black line), nanocage Si–O bond length 1 (blue line), and bond length 2 (orange line). This indicates that there is no phase transition when external strain. Variations in Si-O bonds during the strain process modify the charge density distribution of O atoms, as illustrated in Figs S1–S3. In addition, bond angle 1 (blue line) increases, while bond angle 2 (orange line) decreases.

Under the single-mode relaxation time approximation (SMRTA), lattice thermal conductivity κ_L based on the Peierls–Boltzmann transport theory can be expressed as

$$\kappa_L = \frac{\hbar^2}{k_B T^2 V N_0} \sum_{\lambda} n_\lambda (n_\lambda + 1) \omega_\lambda^2 \boldsymbol{v}_\lambda \otimes \boldsymbol{v}_\lambda \tau_\lambda, \tag{1}$$

where $\hbar$, k_B, T, V, and N_0 are the reduced Planck constant, Boltzmann constant, absolute temperature, primitive unit cell volume, and the total number of sampled phonon wave vectors in the first Brillouin zone, respectively. n_λ, ω_λ, v_λ, and τ_λ are the phonon population, frequency, group velocity, and lifetime for the λ mode (wave vector q and branch index s), respectively.

In Fig. 2(a), lattice thermal conductivity κ_{3ph}^{HA} and $\kappa_{3,4ph}^{HA}$ of 2D-Si_4O_8 with applied strain at 300 K is presented. HA is harmonic approximation. κ_{3ph}^{HA} represents the results considering only three-phonon scattering, while $\kappa_{3,4ph}^{HA}$ corresponds to the results considering both three-phonon and four-phonon scattering. Notably, in κ_{3ph}^{HA} and $\kappa_{3,4ph}^{HA}$, the transition points from an initial increase to a subsequent decrease occur at $\varepsilon = 3\%$ and $\varepsilon = 1\%$ strain, respectively. Therefore, subsequent analyses focus on further examining κ_L for strains of $\varepsilon = 0\%,\ 1\%,\ 3\%,$ and 8%.

κ_{3ph}^{HA} of 2D-Si_4O_8 without strain and $\varepsilon = 1\%,\ 3\%,$ and 8% strain are 28.289, 90.511, 95.755, and 26.297 W m^{-1} K^{-1}, respectively. An increasing trend in κ_{3ph}^{HA} is observed when a small strain is applied, and a decrease in κ_{3ph}^{HA} starts to manifest when the strain reaches 3%. $\kappa_{3,4ph}^{HA}$ under the influence of four-phonon interactions is 1.400, 8.304, 7.490, and 2.848 W m^{-1} K^{-1}, respectively. The inflection point where $\kappa_{3,4ph}^{HA}$ exhibits an initial increase followed by a subsequent decrease occurs at $\varepsilon = 1\%$.

In Fig. 2(b), κ_{3ph}^{HA} and $\kappa_{3,4ph}^{HA}$ of 2D-Si_4O_8 with varying applied strain are depicted, illustrating the relationship with temperatures ranging from 100 to 900 K. As the temperature increases, κ of 2D-Si_4O_8 decreases. $\kappa_{3,4ph}^{HA}/\kappa_{3ph}^{HA}$ reflects the additional influence of 4ph scattering on top of the 3ph process. As shown in Table I, the ratios of $\kappa_{3,4ph}^{HA}/\kappa_{3ph}^{HA}$ indicate 4ph scattering significantly increases the phonon scattering. This suggests that 4ph interactions play an indispensable

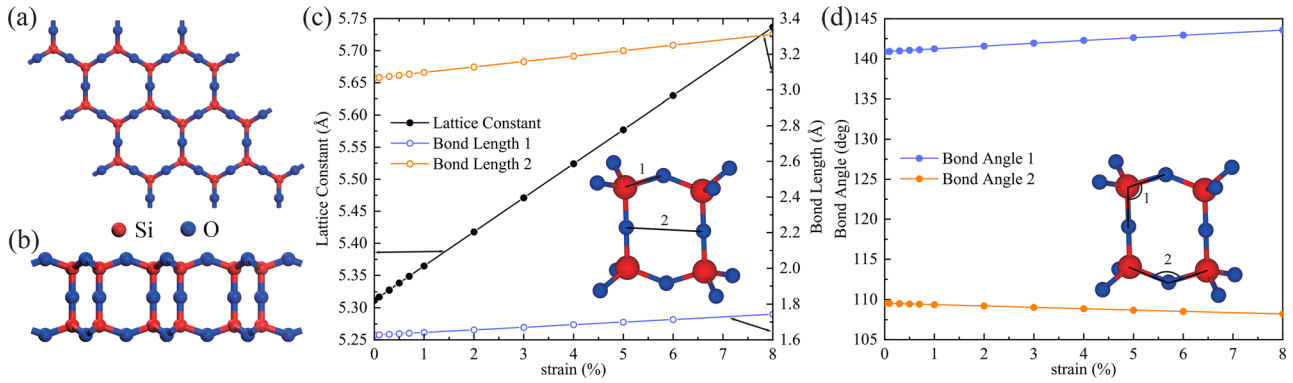

FIG. 1. (a) The top and (b) side views of 2D silica crystal structure without applied strain. Silicon (Si) and oxygen (O) are denoted by red and blue colors, respectively. (c) The lattice constant (left), bond lengths (right), and (d) bond angles as a function of the tensile strain in 2D silica.

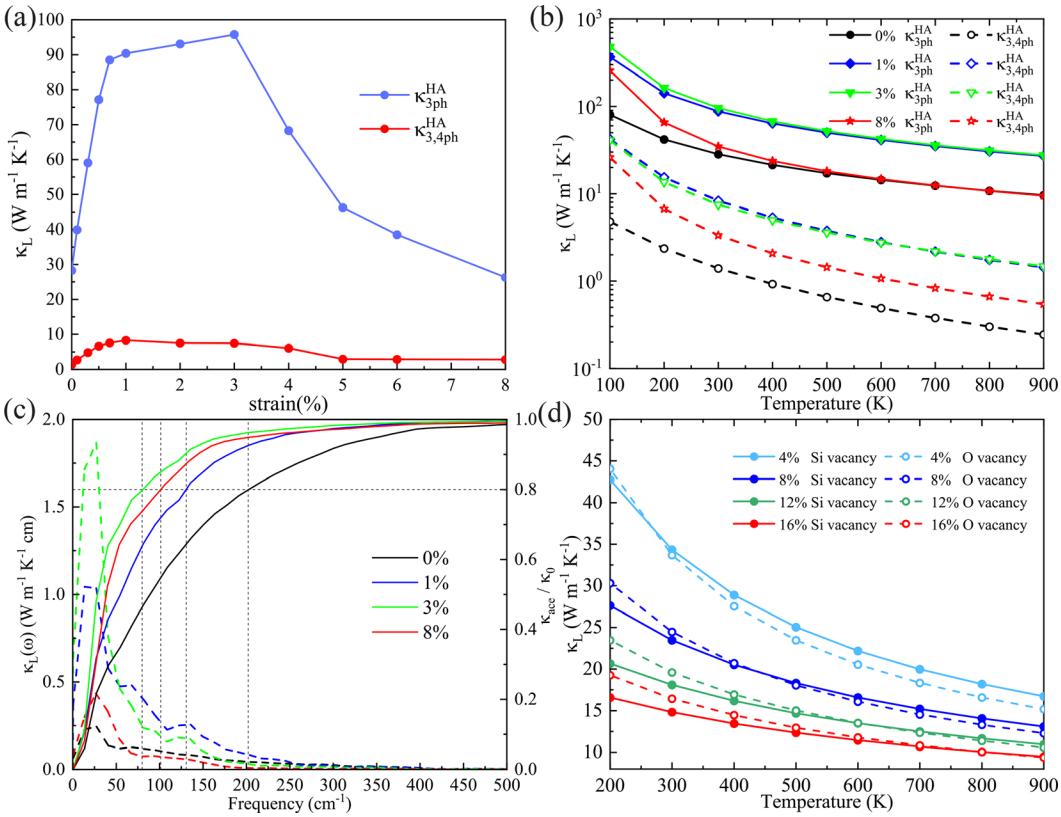

FIG. 2. (a) Lattice thermal conductivity κ_L(W m^{-1} K^{-1}) of 2D-Si_4O_8 with applied strain at 300 K. (b) Two types of thermal conductivity κ_{3ph}^{HA} and $\kappa_{3,4ph}^{HA}$ as a function of temperature for 2D-Si_4O_8 without applied strain and with 1%, 3%, and 8% applied strains. (c) The κ_L spectra and the normalized cumulative κ_{3ph}^{HA} as a function of frequency at 300 K. (d) The effect of Si and O vacancy on κ_{3ph}^{HA} of 2D-Si_4O_8 according to Eq. (2).

TABLE I. The effect of biaxial strain on κ_{3ph}^{HA} and $\kappa_{3,4ph}^{HA}$ and the additional 4ph scattering compared with 3ph scattering in 2D-Si_4O_8.

Strain ε (%)	0	1	3	8
κ_{3ph}^{HA} W m^{-1} K^{-1}	28.289	90.511	95.755	26.297
$\kappa_{3,4ph}^{HA}$ W m^{-1} K^{-1}	1.400	8.304	7.490	2.848
$\kappa_{3,4ph}^{HA}/\kappa_{3ph}^{HA}$	0.049	0.092	0.078	0.108

role in κ_L of 2D-Si_4O_8, highlighting its strong anharmonic characteristics.[15]

To ascertain the causes of the strain-induced variations in κ_L, Fig. 2(c) presents the thermal conductivity spectrum $\kappa_L(\omega)$ and cumulative κ_L curves for 2D-Si_4O_8 under applied strain at 300 K. For 2D-Si_4O_8 without strain, lattice heat conduction is primarily governed by low-frequency phonons and mid-frequency optical branches. These contribute approximately 54% in the range of $\omega = 0$–$100\,\mathrm{cm}^{-1}$ and about 80% in the range of $\omega = 0$–$200\,\mathrm{cm}^{-1}$. As strain increases, the dominance of the low-frequency phonon branch in lattice heat conduction initially rises and then declines.

Given the inevitable formation of vacancy defects during the growth of 2D silica,[38] their impact on κ_L of 2D silica is analyzed. Extrinsic scattering rates due to grain vacancy ($\tau_{d,\lambda}^{-1}$) are calculated by

$$\tau_{d,\lambda}^{-1} = 9\frac{\pi}{2} f_v \omega_\lambda^2 \cdot \mathrm{PDOS}(\omega), \tag{2}$$

where λ represents the phonon mode (q, j) with q and j labeling the phonon wave vector and branch, respectively. f_v represents the concentration of the vacancy. Likewise, ω and PDOS(ω)represents the angular velocities and partial density of states of a basis atom, respectively. The coefficient 9 in Eq. (2) accounts for the mass and bond loss associated with the defect vacancy.[40] Figure 2(d) shows the effects of Si and O vacancies on κ_L of 2D-Si_4O_8. At 300 K, O vacancies significantly reduce κ_L, with the effect of Si vacancies being even greater. For example, when 16% O vacancies are added, κ_L decreases by about 50%. The decreasing trend is more pronounced when increasing Si vacancies and κ_L decreases by about 55%.

The phonon dispersion and PDOS for the strained structure are first calculated, as shown in Fig. 3(a). The absence of imaginary frequencies in the phonon spectrum of strained Si_4O_8 indicates the dynamic stability of the structure. The PDOS reveals a stiffening of the phonon branches with increasing tensile strain. Meanwhile, the low-frequency phonon density of states at 3% strain is anomalously lower than that at 1%.

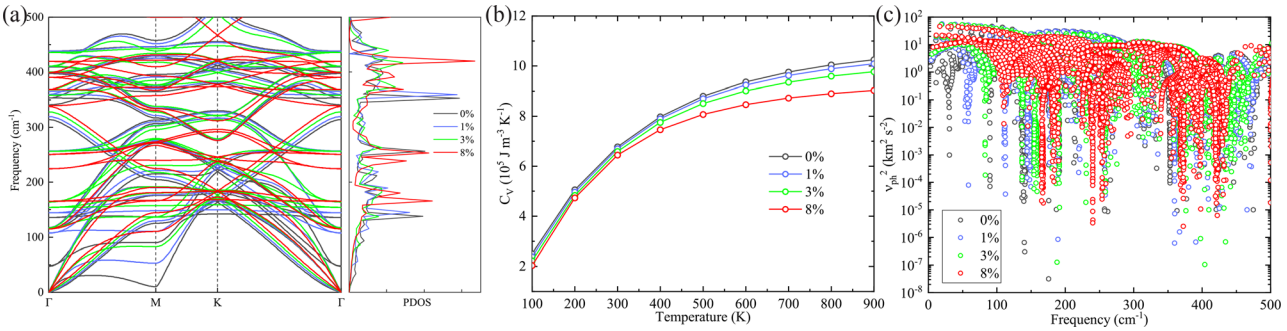

FIG. 3. (a) Phonon dispersions and phonon density of states (PDOS) for 2D-Si_4O_8. (b) Heat capacity C_V as a function of temperature. (c) The square of phonon group velocity v_{ph}^2 at 300 K. The black, blue, green, and red colors represent 2D silica without strain and $\varepsilon = 1\%$, 3%, and 8% strain, respectively.

In Fig. 3(b), the calculated heat capacity (C_V) of 2D-Si_4O_8 is a function of temperature. Derived from C_V, it is evident that κ_L of 2D-Si_4O_8 continuously decreases after the application of strain. This contrasts with the phenomenon observed in κ_L, where an initial increase is followed by a subsequent decrease after strain. In Fig. 3(c), the average phonon group velocity v_{ph} of 2D-Si_4O_8 changes ignorable when the strain increases.

The green curve shows the Ioffe–Regel limit of phonon lifetime τ as a function of phonon frequency ω, represented by $1/\tau = \omega/2\pi$, is plotted. It means that the phonon lifetime τ is equivalent to the vibrational period of a phonon mode. Once the SRs exceed the curve, implying that the phonon lifetime τ is less than one vibrational period, the effectiveness of the phonon quasi-particle picture diminishes. As shown in Figs. 4(a) and 4(b), the majority of 3ph and 4ph scatterings

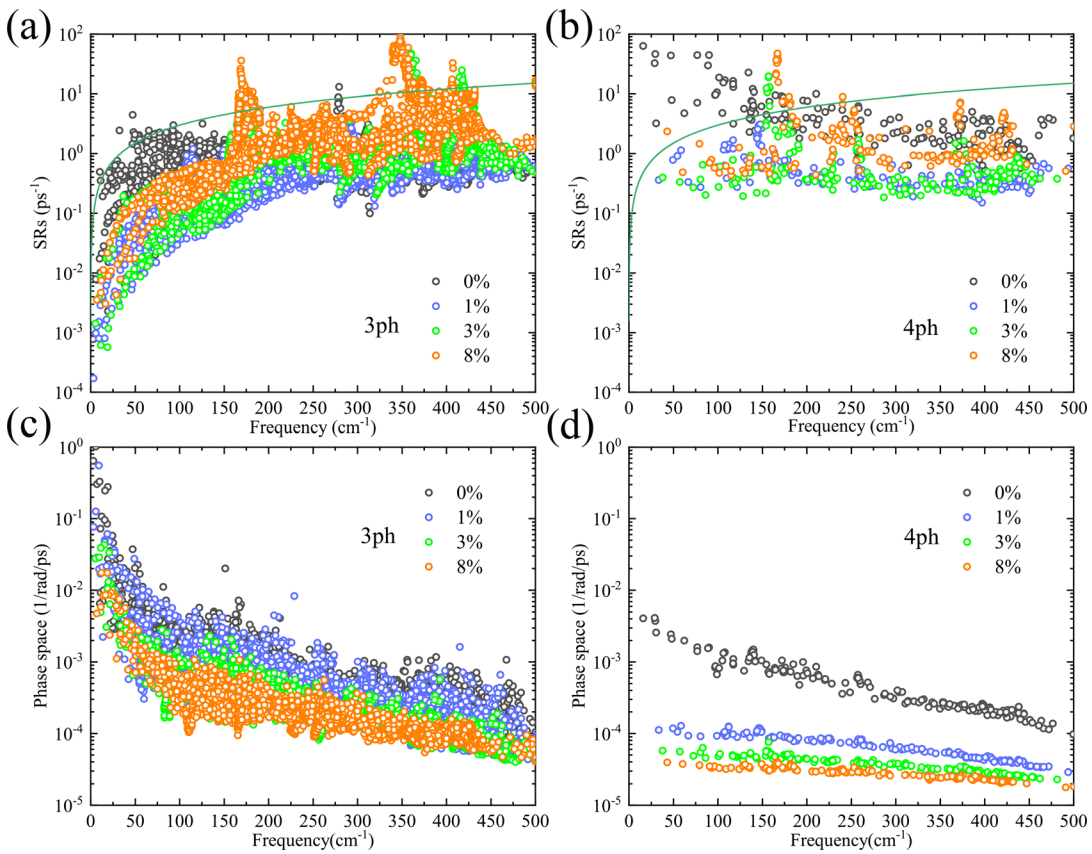

FIG. 4. (a) and (b) Scattering ratios (SRs) and (c) and (d) weighted phase space as a function of frequency of 2D-Si_4O_8 without strain and $\varepsilon = 1\%$, 3%, and8% strain at 300 K. The black, blue, green, and orange colors represent without strain and $\varepsilon = 1\%$, 3%, and 8% strain. 3ph and 4ph represent scattering affected by the harmonic approximation and 4ph scattering affected. The green lines in (a) and (b) indicate the scattering rate is equal to the phonon frequency ($1/\tau = \omega/2\pi$).

are distributed below the $1/\tau = \omega/2\pi$ curve, supporting the validity of the Boltzmann transport equation (BTE) solution in this study.[29,41,42]

Due to the application of different strains, the contribution of various frequency ranges to κ_L varies. As strain increases, there is an initial rise, followed by a decline in the dominance of low-frequency phonons in κ_L. At applied strains of $\varepsilon = 1\%$, 3%, and 8%, approximately 80% of the cumulative κ_L is accounted for at ω around 130, 80, and 100 cm^{-1}, respectively. For the scattering rates of strained 2D-Si_4O_8, there is an initial decrease from without strain to 3% strain, followed by an increase with further strain application. Strain induces reduced scattering rates, enhancing κ_L, aligning with the observed changes in κ_L after strain application in 2D-Si_4O_8.

Under the influence of 4ph scattering, the scattering rate decreases initially from without strain to 1% strain, followed by an increase with further strain application. This corresponds to the observed trend in $\kappa^{HA}_{3,4ph}$, which exhibits an initial rise followed by a subsequent decline. Additionally, the scattering rate for 4ph processes is approximately one order of magnitude higher than that for 3ph processes. This substantiates the significant impact of 4ph interactions on κ_L of 2D-Si_4O_8 with strain.

On the one hand, κ_L initially increases and then decreases as a function of strain, whether considering 3ph or 4ph processes. When tensile strain is applied, the strain-induced flattening of the structure causes the Si–O tetrahedron to deviate increasingly from the standard sp^3 hybridization, as shown in Figs. 1(c) and 1(d). This structural change, driven by small strains, reduces the phonon scattering intensity of the ZA phonon mode (e.g., ZA+ZA → ZA, ZA → ZA+ZA, or TA+ZA → LA/TA). As a result, in Figs. 4(a) and 4(b), the phonon scattering rate for low-frequency acoustic phonons ($<100\ cm^{-1}$) is significantly reduced at 1% and 3% strain compared to the unstrained state, leading to an increase in κ_L. However, for large strains, such as 8% tensile strain, C_V [Fig. 3(b)], v_{ph} [Fig. 3(c)], and τ [Figs. 4(a) and 4(b)] decrease, resulting in a substantial drop in κ_L compared to the smaller strain cases. This behavior is analogous to that observed in monolayer silicene.[43]

On the other hand, the effect of strain on 3ph scattering is more pronounced than on 4ph scattering. This difference arises from the phonon dispersion shown in Fig. 3(a). For acoustic phonons, the frequency increases due to phonon stiffening, while optical phonons soften as a function of tensile strain. This behavior reduces the acoustic–optical (A–O) phonon mode distance, and since each phonon–phonon scattering process must satisfy both quasi-momentum and energy conservation, the A–O phonon mode distance plays a crucial role. Our previous work[44] shows that 4ph scattering is sensitive to this A-O distance. Furthermore, the increased phonon–phonon scattering rate, as shown in Figs. 4(a) and 4(b), also highlights the differing roles of 3ph and 4ph in κ_L. Therefore, the impact of strain is more pronounced in 3ph scattering than in 4ph scattering.

To delve further into the potential mechanisms of phonon scattering, an analysis of 3ph and 4ph phonon scattering phase spaces of 2D-Si_4O_8 at 300 K was conducted, as shown in Figs. 4(c) and 4(d). The results indicate a monotonous reduction in scattering phase space with applied strain, leading to a significant decrease in scattering channels. This reduces the scattering probability, contributing to the elevation of κ_L. Consequently, it emerges as one of the primary factors causing the observed increase in κ_L under small applied strain in 2D-Si_4O_8.

In summary, utilizing first-principles computational methods approach combined with the phonon BTE, we conducted theoretical calculations on strained 2D-Si_4O_8. The obtained κ_L under the influence of 3ph and 4ph interactions was investigated to explore the modulatory effects of applied strain on κ_L of 2D-Si_4O_8. 2D-Si_4O_8 with strain exhibits strong anharmonicity, with 4ph interactions playing an indispensable role in the computation of κ_L. Under strain, the predominant factor influencing the increase in κ_L at small strains is achieved by reducing the phonon scattering phase space and, consequently, lowering the scattering rates. For larger strain magnitudes, the decrease in κ_L is primarily accomplished by an increase in the scattering rates.

Our results elucidate the microscopic heat transfer mechanisms in 2D-Si_4O_8 under applied strain, highlighting the critical influence of lattice strain distribution on κ_L. Additionally, we demonstrate the indispensable role of four-phonon scatterings in determining κ_L of 2D silica. This study may inspire further theoretical and experimental research on strain engineering and substrate effects in materials exhibiting kagome and glasslike κ_L.[30,45–47]

See the supplementary material for the elastic modulus tensor, Young's modulus, differential electron density function, electron distribution density, and electron local function of 2D silica without strain, under 3% strain and under 8% strain.

We acknowledge the support from the National Natural Science Foundation of China (Nos. 12104356 and 52250191) and the Fundamental Research Funds for the Central Universities. This work is sponsored by the Key Research and Development Program of the Ministry of Science and Technology (No. 2023YFB4604100). We also acknowledge the support by HPC Platform, Xi'an Jiaotong University.

AUTHOR DECLARATIONS

Conflict of Interest

The authors have no conflicts to disclose.

Author Contributions

Yang Wang: Data curation (equal); Investigation (equal); Methodology (equal); Software (equal); Writing – original draft (equal). **Xiaoying Wang:** Data curation (equal); Investigation (equal); Software (equal). **Yuzhou Hao:** Data curation (equal); Investigation (equal). **Xuejie Li:** Data curation (equal); Investigation (equal). **Yujie Liu:** Data curation (equal); Investigation (equal). **Jun Sun:** Funding acquisition (equal); Project administration (equal); Supervision (equal). **XiangDong Ding:** Funding acquisition (equal); Project administration (equal); Supervision (equal). **Zhibin Gao:** Funding acquisition (equal); Project administration (equal); Supervision (equal); Writing – review & editing (equal).

DATA AVAILABILITY

The data that support the findings of this study are available from the corresponding author upon reasonable request.

REFERENCES

[1]J. Weissenrieder, S. Kaya, J.-L. Lu, H.-J. Gao, S. Shaikhutdinov, H.-J. Freund, M. Sierka, T. K. Todorova, and J. Sauer, "Atomic structure of a thin silica film on a

Mo(112) substrate: A two-dimensional network of SiO_4 tetrahedra," Phys. Rev. Lett. **95**, 076103 (2005).
[2]D. Löffler, J. J. Uhlrich, M. Baron, B. Yang, X. Yu, L. Lichtenstein, L. Heinke, C. Büchner, M. Heyde, S. Shaikhutdinov, H.-J. Freund, R. Włodarczyk, M. Sierka, and J. Sauer, "Growth and structure of crystalline silica sheet on Ru(0001)," Phys. Rev. Lett. **105**, 146104 (2010).
[3]P. Y. Huang, S. Kurasch, A. Srivastava, V. Skakalova, J. Kotakoski, A. V. Krasheninnikov, R. Hovden, Q. Mao, J. C. Meyer, J. Smet, D. A. Muller, and U. Kaiser, "Direct imaging of a two-dimensional silica glass on graphene," Nano Lett. **12**, 1081–1086 (2012).
[4]P. Y. Huang, S. Kurasch, J. S. Alden, A. Shekhawat, A. A. Alemi, P. L. McEuen, J. P. Sethna, U. Kaiser, and D. A. Muller, "Imaging atomic rearrangements in two-dimensional silica glass: Watching silica's dance," Science **342**, 224–227 (2013).
[5]C. Büchner, Z.-J. Wang, K. M. Burson, M.-G. Willinger, M. Heyde, R. Schlögl, and H.-J. Freund, "A large-area transferable wide band gap 2D silicon dioxide layer," ACS Nano **10**, 7982–7989 (2016).
[6]E. Gao, B. Xie, and Z. Xu, "Two-dimensional silica: Structural, mechanical properties, and strain-induced band gap tuning," J. Appl. Phys. **119**, 014301 (2016).
[7]C. Büchner, S. D. Eder, T. Nesse, D. Kuhness, P. Schlexer, G. Pacchioni, J. R. Manson, M. Heyde, B. Holst, and H.-J. Freund, "Bending rigidity of 2D silica," Phys. Rev. Lett. **120**, 226101 (2018).
[8]Z. Gao, X. Dong, N. Li, and J. Ren, "Novel two-dimensional silicon dioxide with in-plane negative Poisson's ratio," Nano Lett. **17**, 772–777 (2017).
[9]R. Włodarczyk, M. Sierka, J. Sauer, D. Löffler, J. J. Uhlrich, X. Yu, B. Yang, I. M. N. Groot, S. Shaikhutdinov, and H.-J. Freund, "Tuning the electronic structure of ultrathin crystalline silica films on Ru(0001)," Phys. Rev. B **85**, 085403 (2012).
[10]G. Kremer, J. C. Alvarez Quiceno, S. Lisi, T. Pierron, C. González, M. Sicot, B. Kierren, D. Malterre, J. E. Rault, P. Le Fèvre, F. Bertran, Y. J. Dappe, J. Coraux, P. Pochet, and Y. Fagot-Revurat, "Electronic band structure of ultimately thin silicon oxide on Ru(0001)," ACS Nano **13**, 4720–4730 (2019).
[11]G. Kremer, J. Camilo Alvarez-Quiceno, T. Pierron, C. González, M. Sicot, B. Kierren, L. Moreau, J. E. Rault, P. Le Fèvre, F. Bertran, Y. J. Dappe, J. Coraux, P. Pochet, and Y. Fagot-Revurat, "Dispersing and semi-flat bands in the wide band gap two-dimensional semiconductor bilayer silicon oxide," 2D Mater. **8**, 035021 (2021).
[12]L. Lichtenstein, M. Heyde, and H.-J. Freund, "Crystalline-vitreous interface in two dimensional silica," Phys. Rev. Lett. **109**, 106101 (2012).
[13]K. Sun, A. Souslov, X. Mao, and T. C. Lubensky, "Surface phonons, elastic response, and conformal invariance in twisted kagome lattices," Proc. Natl. Acad. Sci. U. S. A. **109**, 12369–12374 (2012).
[14]A. Souslov, A. J. Liu, and T. C. Lubensky, "Elasticity and response in nearly isostatic periodic lattices," Phys. Rev. Lett. **103**, 205503 (2009).
[15]T. Björkman, V. Skakalova, S. Kurasch, U. Kaiser, J. C. Meyer, J. H. Smet, and A. V. Krasheninnikov, "Vibrational properties of a two-dimensional silica kagome lattice," ACS Nano **10**, 10929–10935 (2016).
[16]X. Gu, Y. Wei, X. Yin, B. Li, and R. Yang, "Colloquium: Phononic thermal properties of two-dimensional materials," Rev. Mod. Phys. **90**, 041002 (2018).
[17]H. Bao, J. Chen, X. Gu, and B. Cao, "A review of simulation methods in micro/nanoscale heat conduction," ES Energy Environ. **1**, 16–55 (2018).
[18]G. Fugallo, A. Cepellotti, L. Paulatto, M. Lazzeri, N. Marzari, and F. Mauri, "Thermal conductivity of graphene and graphite: Collective excitations and mean free paths," Nano Lett. **14**, 6109–6114 (2014).
[19]Y. Kuang, L. Lindsay, S. Shi, X. Wang, and B. Huang, "Thermal conductivity of graphene mediated by strain and size," Int. J. Heat Mass Transfer **101**, 772–778 (2016).
[20]X. Zheng, C. Y. Zhao, and X. Gu, "Thermal conductivity of MoS_2/$MoSe_2$ heterostructures: The role of lattice mismatch, interlayer rotation and species intermixing," Int. J. Heat Mass Transfer **143**, 118583 (2019).
[21]J.-W. Jiang, H. S. Park, and T. Rabczuk, "Molecular dynamics simulations of single-layer molybdenum disulphide (MoS_2): Stillinger-Weber parametrization, mechanical properties, and thermal conductivity," J. Appl. Phys. **114**, 064307 (2013).
[22]T. Feng and X. Ruan, "Quantum mechanical prediction of four-phonon scattering rates and reduced thermal conductivity of solids," Phys. Rev. B **93**, 045202 (2016).
[23]T. Feng and X. Ruan, "Four-phonon scattering reduces intrinsic thermal conductivity of graphene and the contributions from flexural phonons," Phys. Rev. B **97**, 045202 (2018).
[24]T. Feng, L. Lindsay, and X. Ruan, "Four-phonon scattering significantly reduces intrinsic thermal conductivity of solids," Phys. Rev. B **96**, 161201 (2017).
[25]Y. Ouyang, C. Yu, J. He, P. Jiang, W. Ren, and J. Chen, "Accurate description of high-order phonon anharmonicity and lattice thermal conductivity from molecular dynamics simulations with machine learning potential," Phys. Rev. B **105**, 115202 (2022).
[26]C. Yu, Y. Hu, J. He, S. Lu, D. Li, and J. Chen, "Strong four-phonon scattering in monolayer and hydrogenated bilayer BAs with horizontal mirror symmetry," Appl. Phys. Lett. **120**, 132201 (2022).
[27]X. Wang, M. Li, M. Feng, X. Li, Y. Hao, W. Shi, J. He, X. Ding, and Z. Gao, "Bonding hierarchy and coordination interaction leading to high thermoelectricity in wide bandgap $TlAgI_2$," Phys. Rev. Mater. **8**, 094601 (2024).
[28]Y. Hao, Y. Zuo, J. Zheng, W. Hou, H. Gu, X. Wang, X. Li, J. Sun, X. Ding, and Z. Gao, "Machine learning for predicting ultralow thermal conductivity and high *ZT* in complex thermoelectric materials," ACS Appl. Mater. Interfaces **16**, 47866–47878 (2024).
[29]Y. Zhao, S. Zeng, G. Li, C. Lian, Z. Dai, S. Meng, and J. Ni, "Lattice thermal conductivity including phonon frequency shifts and scattering rates induced by quartic anharmonicity in cubic oxide and fluoride perovskites," Phys. Rev. B **104**, 224304 (2021).
[30]X. Wang, Z. Gao, G. Zhu, J. Ren, L. Hu, J. Sun, X. Ding, Y. Xia, and B. Li, "Role of high-order anharmonicity and off-diagonal terms in thermal conductivity: A case study of multiphase $CsPbBr_3$," Phys. Rev. B **107**, 214308 (2023).
[31]G. Kresse and J. Furthmüller, "Efficient iterative schemes for ab initio total-energy calculations using a plane-wave basis set," Phys. Rev. B **54**, 11169–11186 (1996).
[32]P. E. Blöchl, "Projector augmented-wave method," Phys. Rev. B **50**, 17953–17979 (1994).
[33]G. Kresse and D. Joubert, "From ultrasoft pseudopotentials to the projector augmented-wave method," Phys. Rev. B **59**, 1758–1775 (1999).
[34]T. Tadano and S. Tsuneyuki, "Self-consistent phonon calculations of lattice dynamical properties in cubic $SrTiO_3$ with first-principles anharmonic force constants," Phys. Rev. B **92**, 054301 (2015).
[35]Z. Han, X. Yang, W. Li, T. Feng, and X. Ruan, "Fourphonon: An extension module to ShengBTE for computing four-phonon scattering rates and thermal conductivity," Comput. Phys. Commun. **270**, 108179 (2022).
[36]Y. Xia, V. I. Hegde, K. Pal, X. Hua, D. Gaines, S. Patel, J. He, M. Aykol, and C. Wolverton, "High-throughput study of lattice thermal conductivity in binary rocksalt and zinc blende compounds including higher-order anharmonicity," Phys. Rev. X **10**, 041029 (2020).
[37]B. Peng, A. Bouhon, B. Monserrat, and R.-J. Slager, "Phonons as a platform for non-Abelian braiding and its manifestation in layered silicates," Nat. Commun. **13**, 423 (2022).
[38]J.-Q. Zhong and H.-J. Freund, "Two-dimensional ultrathin silica films," Chem. Rev. **122**, 11172–11246 (2022).
[39]C. Büchner and M. Heyde, "Two-dimensional silica opens new perspectives," Prog. Surf. Sci. **92**, 341–374 (2017).
[40]B. Xu, T. Feng, Z. Li, S. T. Pantelides, and Y. Wu, "Constructing highly porous thermoelectric monoliths with high-performance and improved portability from solution-synthesized shape-controlled nanocrystals," Nano Lett. **18**, 4034–4039 (2018).
[41]Y. Xia, K. Pal, J. He, V. Ozoliņš, and C. Wolverton, "Particlelike phonon propagation dominates ultralow lattice thermal conductivity in crystalline Tl_3VSe_4," Phys. Rev. Lett **124**, 065901 (2020b).
[42]S. Mukhopadhyay, D. S. Parker, B. C. Sales, A. A. Puretzky, M. A. McGuire, and L. Lindsay, "Two-channel model for ultralow thermal conductivity of crystalline, Tl_3VSe_4," Science **360**, 1455–1458 (2018).
[43]H. Xie, T. Ouyang, É. Germaneau, G. Qin, M. Hu, and H. Bao, "Large tunability of lattice thermal conductivity of monolayer silicene via mechanical strain," Phys. Rev. B **93**, 075404 (2016).

[44]M. Feng, X. Wang, G. Zhu, C. He, J. Sun, X. Ding, J. Shiomi, Y. Xia, B. Li, and Z. Gao, "The relation between the atomic mass ratio and quartic anharmonicity in alkali metal hydrides," Mater. Today Phys. **44**, 101423 (2024).
[45]Y. Pang, J. Liu, X. Fan, H. Yang, J. Zhu, Z. Wang, Y. Yao, X. Qian, and R. Yang, "Glasslike cross-plane thermal conductivity of the kagome metals RbV_3Sb_5 and CsV_3Sb_5," Phys. Rev. B **108**, 205112 (2023).
[46]Z. Tong, A. Pecchia, C. Yam, T. Dumitrica, and T. Frauenheim, "Glass-like transport dominates ultralow lattice thermal conductivity in modular crystalline $Bi_4O_4SeCl_2$," Nano Lett. **23**, 9468–9473 (2023).
[47]R. Cao, Q.-L. Yang, H.-X. Deng, S.-H. Wei, J. Robertson, and J.-W. Luo, "Softening of the optical phonon by reduced interatomic bonding strength without depolarization," Nature **634**, 1080–1085 (2024).